AAS-08-305

# PRECISION ORBIT AND ATTITUDE DETERMINATION FOR ICESAT

**B. E. Schutz[*], S. Bae[**], N. Smith[***], M. Sirota[†]**

The ICESat was launched in January 2003 to detect changes in surface elevation of the polar ice sheets, as well as measure changes in land topography and vegetation cover. The primary instrument carried on ICESat is a single beam laser altimeter (Geoscience Laser Altimeter System). Change detection requires geolocation of the illuminated laser spot on the Earth's surface. Both orbit determination and attitude determination are key components of the geolocation process. This paper reviews the performance of five years in orbit, particularly the experiences in precision attitude determination.

## INTRODUCTION

The global retreat of mountain glaciers has been obvious since the nineteenth century [1]. Even though the melt-water from these glaciers has contributed to the present-day sea level rise of 2 mm/yr [2], the large ice sheets of Greenland and Antarctica contain enough ice to raise sea level by 80 meters if they completely melted. Such complete melting is not imminent, but these ice sheets are expected to exhibit early signs of human-induced climate change. The Ice Cloud and land Elevation Satellite (ICESat) was designed to make direct measurements of temporal surface change of the polar ice sheets.

The primary purpose of ICESat is the determination of inter-annual and long-term changes in polar ice-sheet volume (and inferred mass change) to sufficient accuracy to assess their impact on global sea level [3]. A specific objective of ICESat is to reduce the uncertainty in the known ice-sheet mass balance through determination of polar ice elevation change with better than 2 cm/yr accuracy over 100 km x 100 km areas, averaged over three or more years of seasonal and interannual variability.

ICESat has utilized narrow beam laser altimetry to make the fundamental measurements that lead to the scientific objectives. The hardware carried by ICESat to make these measurements includes the Geoscience Laser Altimeter System (GLAS), which was designed and constructed at NASA Goddard Space Flight Center (GSFC) [16]. GLAS includes other instrumentation that enable generation of the data products necessary to determine ice-sheet surface change. The GLAS payload contains three separate Nd:YAG lasers, each of which was designed to operate with a 40 Hz pulse repetition rate. The

[*] Professor and Associate Director, Center for Space Research, University of Texas at Austin, USA
**Research Scientist/Engineer, Center for Space Research, University of Texas at Austin, USA
***Graduate Student, Center for Space Research, University of Texas at Austin, USA
[†] Sigma Space Corp., Lanham, MD, USA

lasers, pulse optical path, telescope and other instrumentation for the laser operation were mounted on a stable optical bench, as illustrated in Fig. 1. Thermal control has been provided by a system of heat pipes and radiators.

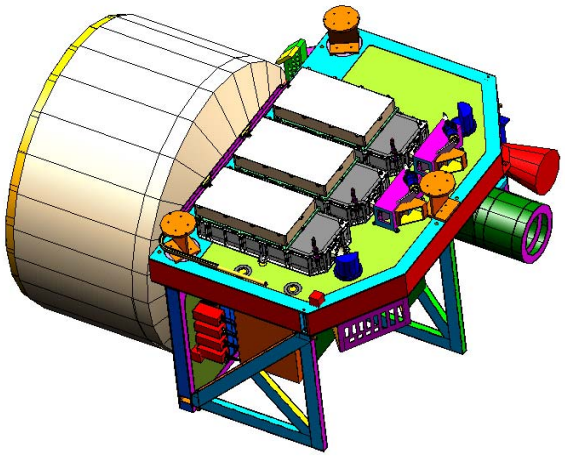

**Figure 1. Depiction of GLAS. The three lasers in identical boxes are mounted on a rigid optical bench; the Sun shade surrounding the one meter telescope is shown on the left. (Diagram courtesy of C. Salerno)**

The GLAS instrument was attached to a commercial spacecraft bus built by Ball Aerospace (Boulder, CO) in June 2002. The ICESat Observatory (or simply ICESat) is shown in Fig. 2 with GLAS attached to the spacecraft bus. Figure 2 shows the nadir side (Earth-facing side) and the zenith side. Thrusters (not shown) used for orbit modification are located on the side opposite the GLAS telescope. Two attitude orientations are used: sailboat mode and airplane mode. In sailboat mode, the velocity vector is parallel to the solar panel rotation axis; in airplane mode, the velocity vector is perpendicular to the solar panel rotation axis.

A Stellar Reference System (SRS) [4] was designed for GLAS with the purpose of providing instrumentation to support accurate attitude determination of the GLAS instrument. The SRS contains an Instrument Star Tracker (IST), a customized star tracker (Laser Reference Sensor, LRS), and a CCD camera to image each transmitted laser pulse, all of which is mounted on the rigid GLAS optical bench. In addition, a Litton Hemispherical Resonator Gyroscope (HRG), is also mounted on the optical bench. The IST and the LRS are Raytheon Optical Systems HD-1003 units. The ICESat real-time attitude determination system uses two Ball CT-602 star trackers mounted on the spacecraft bus (identified as Ball Star Trackers in Fig. 2) with a 60° separation angle between the boresights, the HRG, Sun sensors and magnetometers.

The IST and the two BST cameras operate at 10 Hz with an 8° field of view. The IST tracks up to six stars and each BST tracks up to five stars. The LRS is a modified HD-1003 that operates with an 0.5° field of view at 10 Hz. The LRS typically tracks a single star for the purpose of assessing pointing stability, but it is also used to image the transmit laser pulse and monitor the an optical source known as the Collimated Reference

Source (CRS) mounted on the IST. The CRS, which uses the green channel of the GLAS laser as the light source, was designed to enable monitoring the stability of the IST boresight in the space environment with expected thermal variations of the IST mounting bracket.

Two GPS choke-ring antennas are evident in Fig. 2 in the zenith view, mounted on the spacecraft bus. Each antenna is attached to a JPL BlackJack GPS receiver and only one antenna/receiver set can be operated at a time. A passive laser retroreflector array (LRA) mounted on the spacecraft bus, which supports ground-based satellite laser ranging (SLR), is shown in Fig. 2 in the nadir view.

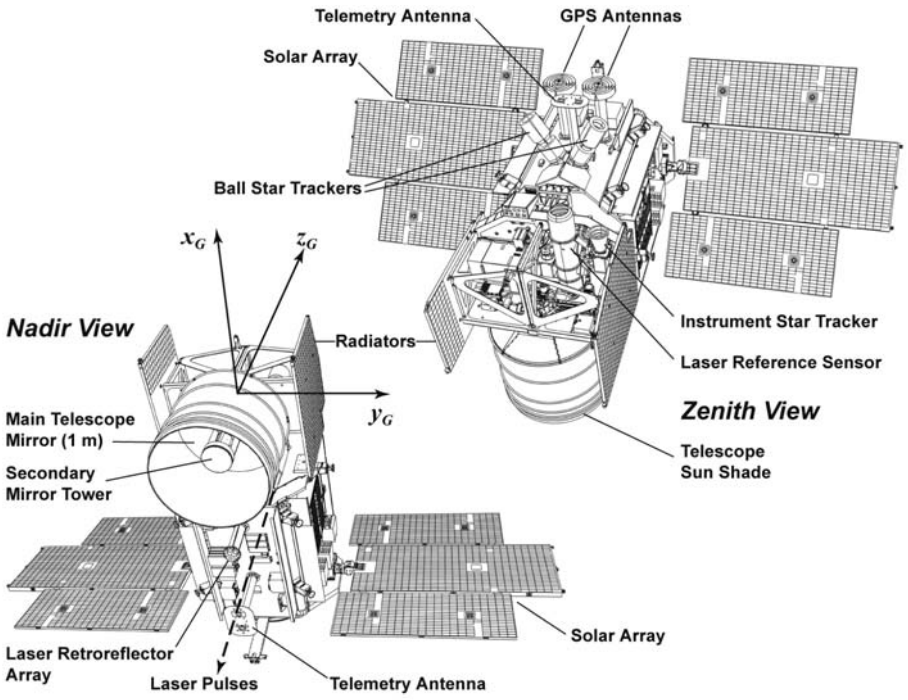


**Figure 2. Nadir and Zenith views of ICESat. The GLAS-fixed axes are denoted as $(x_G, y_G, z_G)$**

## ELEVATION DATA PRODUCT CONCEPT AND IMPLEMENTATION

The 40 Hz operating GLAS laser illuminates a 65 m diameter spot (or footprint) in near infra-red (1064 nm) on the Earth's surface as illustrated in Fig. 3. Successive spots produce a sequence of ground spots, or "spot track", on the surface, with a spot separation of ~172 m, determined by the 40 Hz pulse repetition rate, the orbital motion and the Earth rotation. The transmitted 1064 nm laser pulse from GLAS illuminates a spot on the surface and the echo pulse (the reflected photons) is captured by a 1 meter diameter telescope and directed to an analog detector, then digitized by a 1 GHz sampler, which also digitizes the transmit pulse. The approximately 8 millisec roundtrip time of flight (TOF) for the transmitted photons to return to the GLAS instrument are precisely determined from the transmitted pulse can be determined from the digitized transmit and

echo waveforms. The one-way range, or magnitude of the range vector ($\mathbf{H}$), is half the TOF multiplied by the speed of light. Using the IST and HRG and other instrumentation, the directional information of the range vector is determined.

The position vector of a GLAS reference point is determined from analysis of measurements collected by the operating GPS receiver. Since January , 2003, only Flight Model (FM) #1 has been in operation (in Figure 2, the antenna for FM#1 is the left-most antenna in the zenith view). The ICESat ephemeris resulting from this analysis is further validated using the SLR measurements acquired using the LRA and the ephemeris provides the time-dependent position vector $\mathbf{R}$ in the adopted International Terrestrial Reference Frame (ITRF), most recently identified ast ITRF-2005, a realization of an Earth-centered, Earth-fixed reference system with origin coinciding with the Earth's center of mass. The geolocated illuminated laser spot is determined from

$$\mathbf{R}_{spot} = \mathbf{R} + \mathbf{H} \tag{1}$$

The process whereby the position vector $\mathbf{R}$ is determined is referred to as "precision orbit determination" (POD). The process whereby the direction of $\mathbf{H}$ (the range vector, or altitude vector) is determined is referred to as "precision pointing determination" (PPD); the magnitude of $\mathbf{H}$ is determined from the TOF as described above. An important component of the PPD is the "precision attitude determination" (PAD), which determines the spatial orientation of the GLAS optical bench, i.e., the spatial orientation of the $(x_G, y_G, z_G)$ axes. In other words, PPD consists of PAD plus knowledge of the laser direction with respect to the GLAS-fixed axes. Special maneuvers, known as Scan Maneuver Calibrations, are performed over the ocean to provide calibrations of the laser $\mathbf{R}$ direction and to validate the PPD [5]. The position of the illuminated spot, $\mathbf{R}_{spot}$, can be expressed in the appropriate ITRF or transformed to geodetic latitude, longitude and ellipsoid height. The primary data product used to detect ice sheet surface change, for example, is the geolocated illuminated spot, namely, $\mathbf{R}_{spot}$, particularly the ellipsoid height, or elevation, component of the geodetic coordinates. Hence, the "elevation data product" encompasses $\mathbf{R}_{spot}$.

The prelaunch accuracy requirements for $\mathbf{R}_{spot}$ were expressed in terms of requirements for $\mathbf{R}$ and $\mathbf{H}$. The requirement for $\mathbf{R}$ was 5 cm (1 σ) in the radial direction and 20 cm in the horizontal direction (along-track and cross-track components). The requirement for the direction of $\mathbf{H}$ was 2 arcsec, or an inferred horizontal spot location on the surface of 6 m. The POD process and the PAD process provide the respective vectors in the International Celestial Reference Frame (ICRF), which is closely aligned with the usual mean equator and equinox of J2000. However, the result for $\mathbf{R}_{spot}$ is required in an Earth-centered, Earth-fixed frame, currently realized with the ITRF-2005 (International Terrestrial Reference Frame). The coordinate transformation between the ICRF and the ITRF is applied, which is dependent on precession, nutation, polar motion and UT1 (e.g., see Appendix H of [6]).

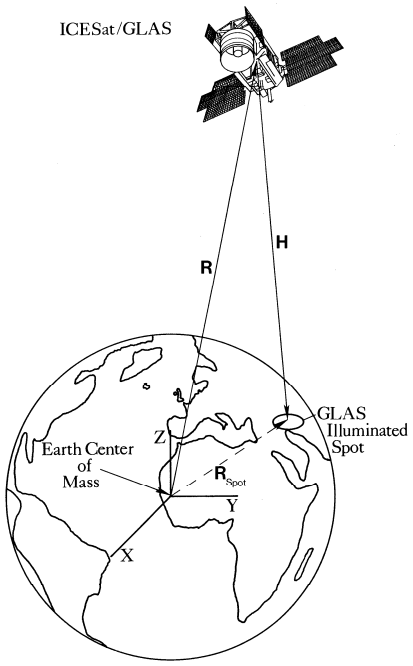


**Figure 3. Determination of laser illuminated spot coordinates (ICESat elevation data products)**

## MISSION DESCRIPTION

ICESat was launched January 13, 2003, 00:45 UTC on a Boeing Delta-II from Vandenburg AFB. The required near-circular, frozen orbit with an altitude of approximately 600 km and an inclination of 94° was achieved with little dispersion at the planned orbit insertion. The launch orbit had a repeating ground track with a period of 8-days, which was determined to support repeated overflights of calibration/validation sites. An overview of the mission is available [7].

Laser #1 was activated in February 20, 2003, and failed in March 29, 2003. A GSFC review board carefully examined the failure and made recommendations for the operation of the two remaining lasers. A modified operating plan was adopted that called for approximately 30-day operation periods, three times per year, to enable a time series of measurements in support of the science objectives. Laser #2, which was activated September25, 2003, exhibited a faster than expected energy decay and has not been operated since June, 2004. Laser #3 has been operated for regular 33 day periods, two or three times per year, and was most recently operated in March, 2008, and the planned next operation period is October, 2008.

As of this writing, the best available laser pointing calibrations from SMC have been introduced and the elevation data products, referred to as Release 428 are available from National Snow and Ice Data Center (NSIDC). In addition, the IST, BST, HRG and LRS

data are available (data product GLA04). In the designation "Release 428", the number 4 denotes the level of pointing accuracy and the number 28 represents the release number associated with the data products. It should be noted that Release 29 is in preparation. The NSIDC web site provides information about the characteristics of Release 28.

## POD PERFORMANCE

ICESat POD is based on analysis of the GPS data from FM#1. The POD uses the GPS carrier phase data recorded by FM#1 in a double-difference (DD) mode (i.e., the ICESat carrier phase data are differenced with a subset of receivers from the International GNSS Service (IGS) network. The POD uses a batch dynamic approach in which the IGS GPS ephemerides (final IGS version) are fixed and various parameters for the ICESat orbit are estimated, including DD phase biases, epoch state, drag and radiation pressure coefficients, and zenith delay. The GRACE gravitational model GGM01C [8] was adopted and the POD software was the CSR TEXGAP package, which includes MSODP [9].

The solution strategy uses a batch period of 30-hours. The central 24-hours are reported as the POD product and the remaining 6-hours (3-hours on both ends of the arc) are used to compare with the ephemeris product for the preceding arc and the following arc. This comparison is referred to as the overlap and the statistics are a useful validation of the POD product, although it usually provides an optimistic assessment of the POD accuracy. For all ICESat campaigns through March 2008, the 3-dimensional RSS is less than 2 cm for the overlaps. A more robust assessment can be obtained by using the GPS-determined orbit with the SLR data and generating SLR residuals. Examination of the high elevation SLR residuals (> 60°) provides a good approximation to the accuracy of the radial component of the orbit. In this case, the high elevation residuals give an RSS of less than 2 cm over all operation periods. Only one 33-day campaign produced an RSS that exceeds 2 cm (namely, one case with 2.5 cm). Hence, it is concluded that the POD exceeds the POD requirement with a radial accuracy assessment of ~ 2 cm.

## PAD PERFORMANCE

The PAD methodology is based on the application of an Extended Kalman Filter (EKF) to the IST, LRS and gyro data, including techniques for star identification. As part of the quality control, a single frame attitude determination of quaternions is performed based on the QUEST algorithm [11], but these quaternions are not input to the EKF processing. The estimation algorithm for the EKF [12] provides the attitude quaternions based on the star tracker and gyro data.

The elevation data product identified as level 428 has achieved the required pointing knowledge 1-$\sigma$ accuracy of 2 arcsec (i.e., the local horizontal geolocation accuracy is ~ 6 m). This accuracy has been validated, for example, at the White Sands (NM) ICESat Cal/Val Site as described in [13]. Various challenges had to be addressed in order to achieve the pointing accuracy requirements exhibited by Rel. 428. Of particular importance, as previously noted, was the pointing corrections derived from Scan Maneuver Calibrations, described in [5]. However, a variety of characteristics surfaced in the PAD area, some that were expected and some that were unexpected, that needed to be addressed in order to achieve the pointing knowledge requirement. In some cases, new methodology had to be developed and in other cases, new corrections were obtained. In

general, it is thought that many of the observed effects could contribute to the planning and operation of future missions. These characteristics are summarized in the following sections.

*Motion of the IST*

The LRS was designed to monitor the stability of the IST mounting bracket since pre-launch studies suggested the possibility of significant bracket motion in response to thermal effects. The CRS was rigidly attached to the IST bracket and designed to emit pulses at 10 Hz that are imaged in the LRS. On-orbit data show a periodic IST bracket motion with an overall variation of about 20 arcseconds and a period of one orbital revolution, as shown in Figure 4, obtained during the initial operation of Laser 2. The characteristics of this orbital variation vary with the thermal and mechanical configuration. Since this sensor shows a motion of the IST with respect to the GLAS reference frame, attitude estimates based on raw IST data contain this orbital variation, in addition to any other alignment variations. In other words, motion of the IST produces an apparent attitude variation of the GLAS optical bench. In this case, however, the CRS data was used to correct the IST data before attitude estimation, which significantly improved PAD and PPD for the laser 2 operation period in October 2003 [14].

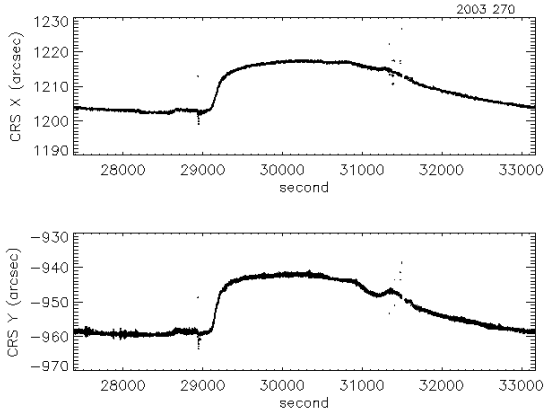


**Figure 4. CRS Motion for One Orbital Period on October 9, 2003**

The CRS signal uses the GLAS green laser energy, which exhibited a significant lower energy in the operation periods beginning in 2004. In fact the CRS became unobservable by October 2004. A *batch-EKF correction* method was developed to replace CRS data; it compares a batch attitude estimate and an EKF attitude estimate [15]. The batch method estimates an attitude quaternion and gyro biases at the epoch time of the batch interval; the batch interval is one orbital period. Using the bias-corrected gyro data, the attitude is propagated from the epoch time to the end of the batch interval. The propagation does not involve IST data so the attitude estimate is not affected by IST alignment variation. Subtracting the batch attitude from the EKF attitude provides information similar to the CRS data. This *batch-EKF curve* is used to correct the IST data. Corrected IST data is then used for a final EKF attitude estimation.

This batch-EKF correction has been used for PAD and PPD for all laser operation periods except the first laser 2 operation period. Figure 5 shows the batch-EKF curve for one orbital period and corresponds to the CRS curve shown in Figure 4; the curves are similar. Although the batch method is not affected by IST alignment variation, it is sensitive to attitude maneuvers. For large maneuvers the batch estimate error can grow to

tens of arcseconds, while the EKF estimate error remain small. To reduce the effect of maneuvers, good batch-EKF curves are selected daily; one smoothed curve is derived and used repeatedly for the whole day.

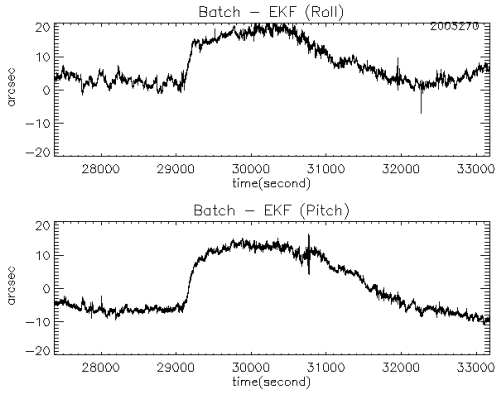


**Figure 5. Batch-EKF Curve for one Orbital Period on October 9, 2003**

*Time Reversals and Data Duplicates*

Early in the mission IST time reversals and data duplicates impeded the PAD/PPD processing or caused large errors in the attitude estimates. In a time reversal the data time-tags are not in increasing order. In a data duplicate the data is the same at successive time-tags. These problems were caused by the star tracker center of integration time data being out of the expected range. The ground software which converted raw IST data to a user-friendly data format was modified to correct these problems. This modification introduced frequent short time-tag skips in the IST data of mostly 0.1 second length. For example, there were 36580 time-tag skips over the 24 hours on June 8, 2008. These time-tag skips were corrected using rate information from the gyro data. Another issue was valid IST stars that show inappropriate movement over time; preprocessing of the IST data removes these stars.

The specification output rate for all of the star trackers was 10 Hz. When the time-tags from all of the instruments were compared, the IST output rate showed discrepancies as in Figure 6. The IST output rate was slightly less than 10 Hz. IST data essentially links the optical bench attitude to the Celestial Reference Frame, so PAD/PPD processing is interpolated to the IST measurement times.

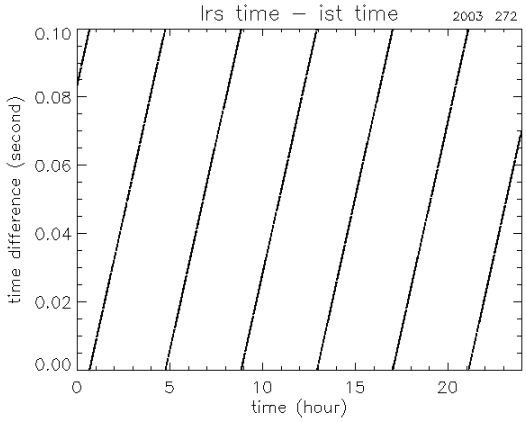


**Figure 6. Time-Tag Differences Between LRS and IST for October 11, 2003**

*IST Time-Tag Shift*

During the laser 3 campaign in June 2005 the daily bias averages in the ocean data analysis showed anomalous numbers in several days; the IST raw data had 0.1 second time-tag shifts for one or a few orbits. This problem also occurred in sailboat mode periods a few times over the length of the mission. It occurred much more frequently in airplane mode, especially in the June 2005 laser 3 campaign.

The left plot in Figure 7 shows the quaternion differences between IST attitude and BST2 attitude during a day in June 2005 laser 3. There is a discontinuity (or jump) from the mean value at the beginning of the day and in the middle of the day. The jumps start and end during the IST sun-blinding periods and usually last one or two orbital periods.

A similar discontinuity is seen in the sailboat mode cases. Sailboat mode IST to BST1 boresight direction difference is shown in the right plot of Fig. 7. The size of the discontinuity in this plot is around 22 arcseconds which corresponds to the 0.1 second change in the relative geometry between the star trackers and the ICESat velocity direction. Correcting the IST time-tags by 0.1 seconds removes the discontinuities from the difference plots as shown in Fig. 8.

The cause of the IST time-tag shifts is not known. In airplane mode the shifts occur during IST sun-blinding when there is no data. In sailboat mode 200 second data gaps are always found before and after the shift.

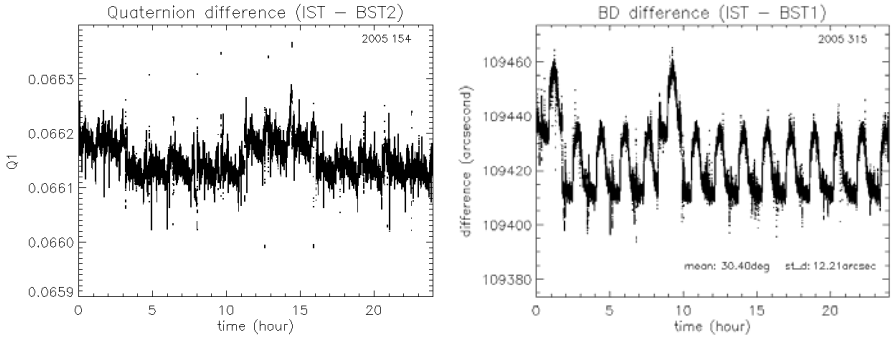


**Figure 7. IST quaternion – BST2 quaternion (June 3, 2005) and IST BD – BST1 BD (November 11, 2005)**

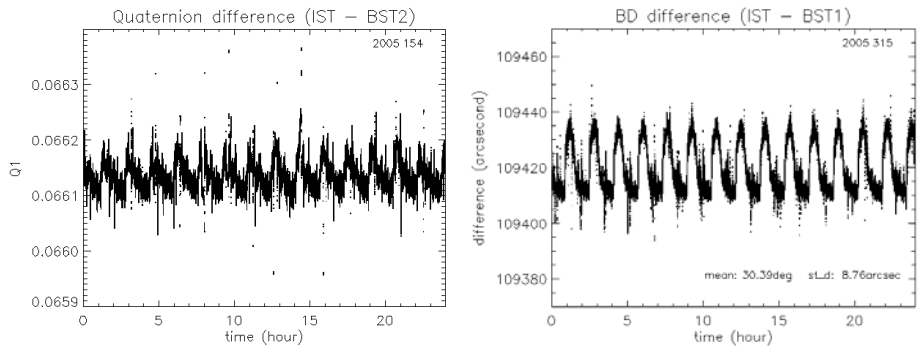


**Figure 8. IST quaternion – BST2 with the fixed IST data (June 3, 2005) and IST BD – BST1 BD with the fixed IST data (November 11, 2005)**

*HRG Time Tag*

Analysis of the ICESat surface elevation products from Salar de Uyuni in Bolivia showed a 2.8 Hz signal, but this characteristic did not exist in the surface topography. Examination of the gyro data showed that it was about 50 milliseconds out of phase, based on comparison with the LRS star motion. The left plot of Figure 9 shows the gyro angle with respect to the LRS star movement angle along corresponding axes; the RMS of this difference for various gyro time-tag shifts is shown in the right plot. The 2.8 Hz oscillation over the Bolivian dry lake was reduced when the gyro time tag was adjusted by 50 milliseconds with respect to the LRS and IST. The 50 milliseconds might not be the precise number and may vary with time and temperature, but the remaining effect of gyro time-tag shifts on the elevation products has been negligible.

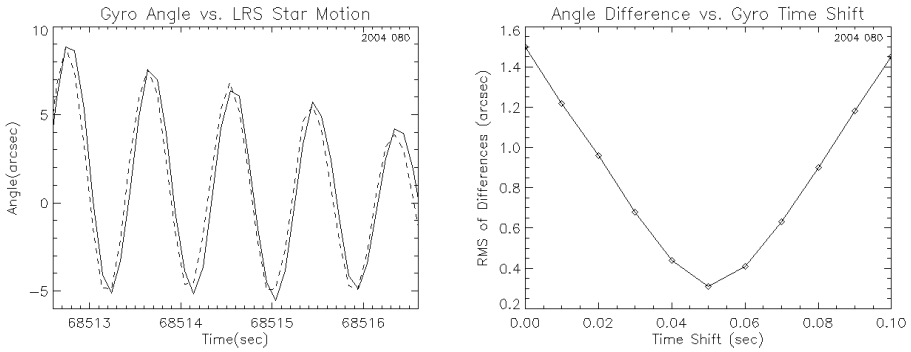


**Figure 9. 50 Millisecond Gyro Angle Bias with Respect to the LRS Star Motion and RMS of Angle Differences Between Gyro and LRS for Various Gyro Time-Tag Shifts**

At the beginning of the mission the gyro time-tags were based on the external Bus Vehicle Time Code Word (BVTCW); this data should have a reliable 10 Hz frequency, but introduced a gyro rate signal with a period of approximately 220 second, as shown on the left in Figure 10. This problem was solved by using the free-wheeling internal clock of the gyro, directly associated with the angle measurements, as shown in the right plot.

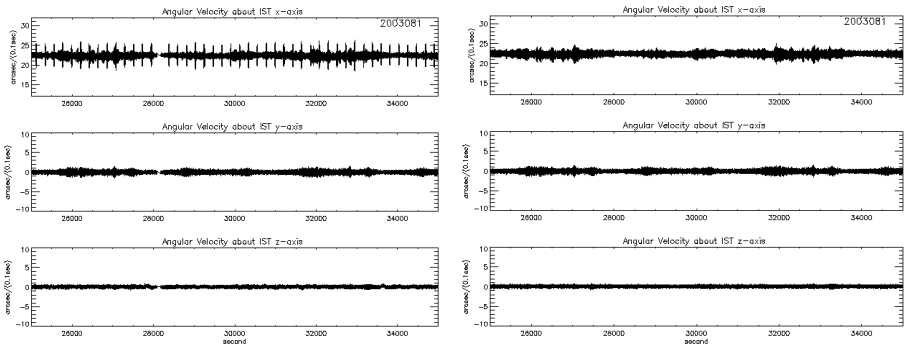


**Figure 10. Gyro Rates in the Three IST Axes Using the BVTCW (Left) and the Gyro Clock (Right)**

Using the gyro clock results in a drift of the EKF attitude estimates with respect to the QUEST estimates, as shown in Figure 8; the QUEST method does not use gyro data (Shuster 1981). The drift is caused by the gyro clock's slightly faster rate; no drift is seen if the BVTCW is used. Synchronizing the gyro clock to the BVTCW introduces occasional gyro data gaps; these gaps add up to a few seconds each day. A scale factor is used to correct the gyro date by stretching it to cover an 86200 second day.

EKF attitude estimates using corrected gyro data do not show a drift with respect to the QUEST estimates, as shown in Figure 11. The magnitude of the correction varies from day to day, possibly because of variations in the optical bench temperature; during abrupt thermal variations the scale factor changes rapidly.

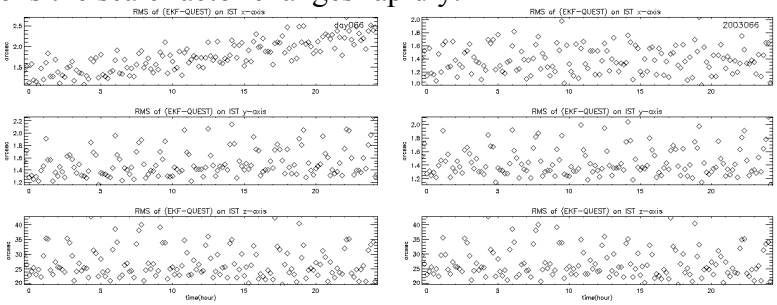


**Figure 11. Drift of EKF Attitude Estimates with Respect to QUEST Estimates Before (Left) and After (Right) Gyro Clock Correction**

*IST Sun-Blinding*

During June airplane mode campaigns there is a period during which the IST experiences Sun-blinding. For example, laser 3 campaign that lasted 33 days from May 20 to June 23 in 2005. At the beginning of the campaign the Sun-blinding data gaps were about 400 seconds and the beta prime angle, the angle between IST bore-sight direction and the Sun, was -20°; at the end of the campaign the data gaps were about 750 seconds and the beta prime angle was -4°.

During IST sun-blinding PAD/PPD is based solely on gyro data and attitude errors can grow to tens of arcseconds. Figure 12 shows the attitude error calculated by differencing the PAD/PPD attitude and the BST2 attitude for one orbital period in June 2005 Laser 3; the deviation at the center of the period is caused by IST sun-blinding. Since PAD/PPD target the polar regions sun-blinding at low latitudes should not be a practical problem, but one of the two daily ocean scans occurs during sun-blinding.

The simplest solution to sun-blinding is to use data from BST1 and BST2, but they are pointed 30 degrees away from the zenith and their yaw uncertainty is introduced into PAD/PPD. The following batch estimation method is a better solution:

1. Apply the Batch-EKF correction to the IST data
2. Determine the attitude with EKF from the corrected IST data
3. Determine the attitude with 15-state batch method from the corrected IST data
4. Use the EKF attitude for PPD except in the sun-blinding periods
5. Replace EKF attitude with 15-state batch method attitude in the sun-blinding periods

For the batch-EKF correction, we have used a 6-state batch method that determines three attitude error quaternion and three gyro rate biases. The 15-state batch method additionally estimates gyro characteristics such as misalignment error and scale factor error. It is important that the 15-state batch method be applied to batch-EKF corrected IST data, and only be used in the sun-blinding periods. The 15-state batch method and corrected IST data reduce the attitude error deviation to a few arc seconds, as shown on the right in Figure 12.

Unlike other targeting maneuvers, the ocean scan maneuvers rotate ICESat for relatively long periods of about 20 minutes over a 3 to 5 degree radius. The attitude accuracy during sun-blinding and an ocean scan maneuver are still not sufficiently good for the normal laser ranging analysis, but the improvement using the 15-state batch method is noticeable. Further research to improve batch method performance during ocean scans is currently underway.

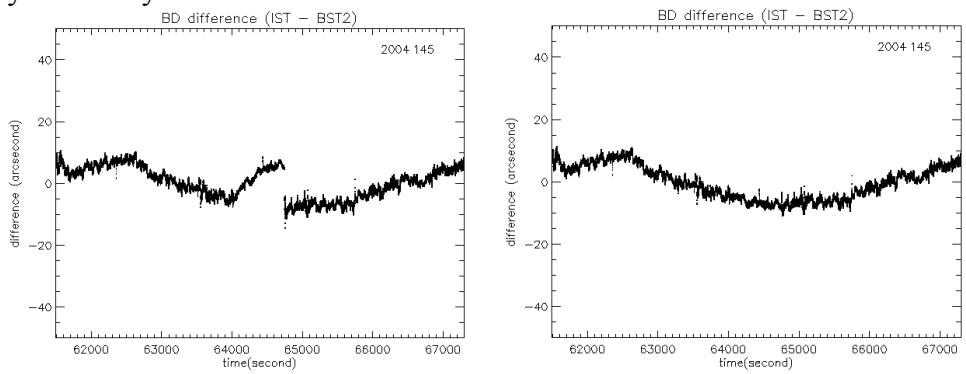


**Figure 12. Comparison of PAD/PPD and BST2 Attitude Estimates for One Orbital Period Showing the Deviation Due to Sun-Blinding (Left) and the Performance of the 15-State Batch Method Correction**

*Star Brightness and Noise Dependence*

Star tracker measurement noise is estimated from multiple measurements of three or more stars. The variance of the measured angle between a pair of stars equals the sum of the star variances. For three stars, the three possible pairings provide three equations with the three star variances as unknowns. For more than three stars the system is over-determined and the measurement variances are solved for using least squares. Figure 13 shows IST measurement noise as a function of star magnitude. Similar plots for BST1 and BST2 show the same structure shifted slightly downward to lower noise levels.

Structural shifts upward due to scattered light from the Sun and Moon are currently being studied. These noise estimates can be used for weighting of the star measurements used in attitude estimation. Each point represents a pass of a star through the star tracker field of view; there are a total of 1214 passes for 227 stars. A pass is usually 50 to 150 seconds long (500 to 1500 frames) and a star is usually paired with 5 to 10 other stars in a pass. The vertical axis is the square root of the star variance calculated using the Singular Value Decomposition form of the least squares solution.

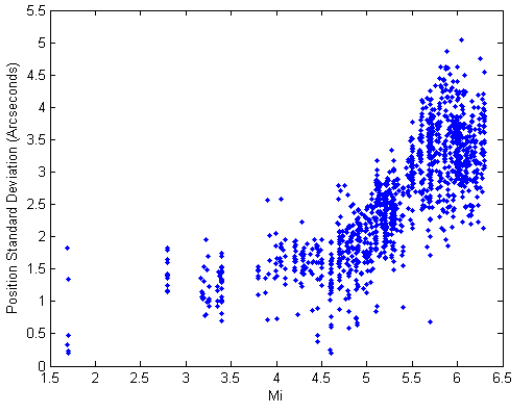


**Figure 13. IST Measurement Noise vs. Star Magnitude**

*Star Tracker Distortion*

A star's predicted position can be calculated given an estimate of the star tracker attitude; the star's position residual is the difference of its measured and predicted position. Distortion is a pattern of position residuals across the field of view that is nearly constant in time. Figure 14 shows the magnitude of the additive correction that minimizes the sum of the squares of the position residuals for the IST. Plots for BST1 and BST2 are similar. The effect of distortion correction on overall ICESat PAD and PPD is small. The IST field of view is 8 by 8 degrees and the correction is a function of third degree polynomials in the horizontal and vertical coordinates. About three million star measurements were used in the least squares solution; 3 revs each from 6 days in September-November 2003 and 8 days in October-November 2004. The days selected were at least 5 days apart to increase coverage of the field of view.

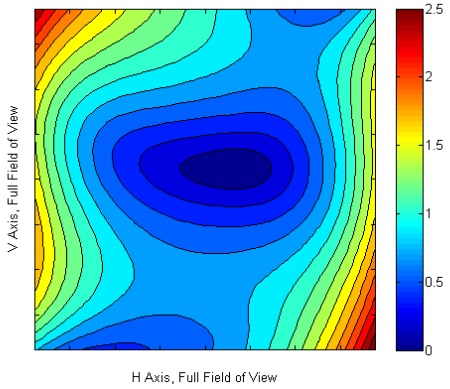


**Figure 14. IST Distortion Magnitude (Arcseconds)**

*Biased Star Positions*

Near neighbor stars and transient objects can bias star centroiding. An IST pixel covers about 58 arcseconds so bright objects within a few arcminutes of a catalog star are potential problems. Some star catalogs reduce the effects of near neighbor stars by giving blended positions. Automated detection and classification software is being used to study star biases. Figure 15 shows an example of a catalog star with a position bias due to a near neighbor. The left plot shows the mean measured positions of Hipparcos catalog star number 46509 (HIP 46509) relative to its predicted position. 18 passes of HIP 46509 are shown: 6 IST, 6 BST1, 6 BST2. The along track axis is the direction of motion tracking of the star through the star tracker field of view; this direction is approximately north-south for ICESat. On the right is a photo of HIP 46509 from a ground based telescope, HIP 46509 and the bright near neighbor have visual magnitudes of 4.6 and 7 (this research has made use of Aladin and the SIMBAD database, operated at CDS, Strasbourg, France). We are working under the assumption that about 1% of catalog stars may have biased positions. The effect on overall ICESat PAD and PPD is small, but we are data mining the ICESat star tracker data to characterize the problem and improve future mission star catalogs.

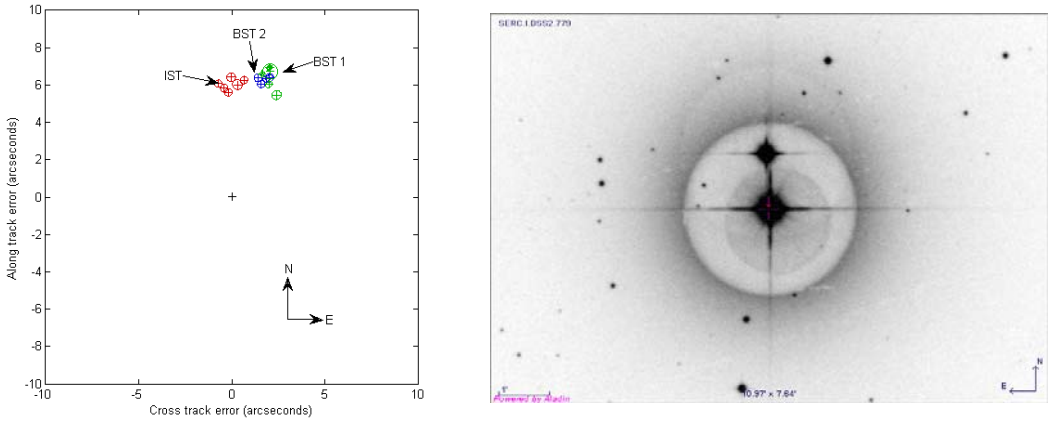


**Figure 15. HIP 46509 Position Bias**

*High Frequency Star Centroiding Error*

High spatial frequency error is primarily caused by faulty centroiding as stars moves across pixel boundaries. Stars cross IST pixels in the along track direction at a frequency of 3.8 Hz; this signal is shown in Figure 16, a plot of the power spectral density of the along track position residuals. The signal peak is reproduced by a simulation sinusoidal signal with a frequency of 3.85 Hz and a peak-to-peak amplitude of 2.2 arcseconds. The vertical axis was rescaled to show the sinusoid amplitude based on the simulation. The frequency of 3.85 Hz is validated by a calculation of the angular width of the IST field of view based on an orbital period of 96.5 minutes and a CCD width of 512 pixels; the calculation results in an angular width of about 8 degrees, which agrees with the IST specification.

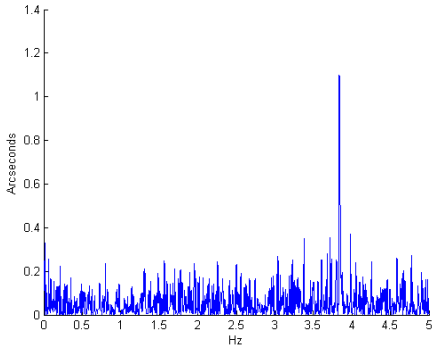


**Figure 16. IST High Spatial Frequency or Pixel Frequency Error Power Spectral Density for Along Track Position Residuals of a Mi 4.7 Star (Rescaled to Arcseconds)**

*IST Lightshade Performance*

Each summer there is a period when the sun passes directly through the IST field of view. IST lightshade performance for one orbit is shown in Figure 17. The IST outputs background counts for each of the six virtual trackers and the mean value is shown as function of angle between the boresight and the Sun. The orbit shown is from June 10, 2003 when the beta prime angle was -0.2 degrees; the sun passed nearly directly through the IST boresight. We are studying the effects on the star tracker noise of the increasing scattered light represented by the curve between 90 degrees and about 20 degrees.

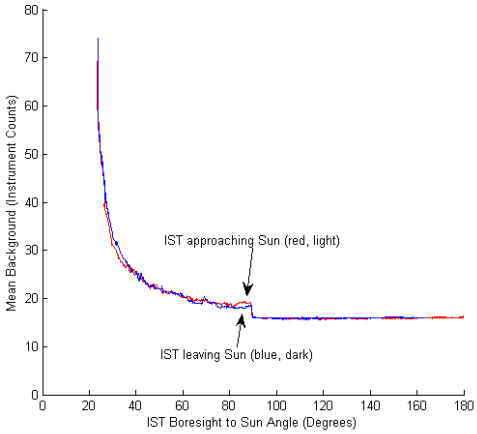


**Figure 17. IST Background Counts during a Sun Transit**

## CONCLUSIONS

ICESat has completed more than five years in orbit. The satellite has four star trackers and a high performance gyro system, plus two GPS receivers, to meet the high precision orbit and attitude determination requirements. These requirements have been met with the Release 428 level of the elevation data products. However, a variety of effects have been experienced during the five years in orbit and, in some cases, methodologies to accommodate unexpected characteristics have been developed as described in this paper. The effects on Precision Attitude Determination that have been described are: motion of the IST caused by thermal variations over an orbital revolution, time reversals and data

duplicates, IST time-tag drift, HRG time tag, IST Sun-blinding, star brightness and noise dependency effects, star tracker distortion, biased star positions, high frequency star centroiding errors and IST lightshade performance. The ICESat data used for PAD are available from the NSIDC in the GLA04 data files. The observed on-orbit characteristics provide fundamental understanding of the instruments, which can contribute to the design of future missions.

## ACKNOWLEDGEMENTS

The final IGS ephemerides have been used in this paper and the services provided by IGS, the International Laser Ranging Service and the International Earth Rotation Service are gratefully acknowledged.

## REFERENCES

[1] Houghton, J., L. Filho, B. Callander, N. Harris, A. Kattenberg and A. Maskell, *Climate Change 1995: The Science of Climate Change*, Cambridge University Press, 1996.

[2] Nerem, S., B. Haines, J. Hendricks, J. Minster, G. Mitchum and W. White, Improved determination of global mean sea level variations using TOPEX/POSEIDON altimeter data, *Geophys. Res. Letters*, V. 24, No. 11, 1331-1334, June 1, 1997.

[3] Zwally, J., et al., ICESat's laser measurements of polar ice, atmosphere, ocean and land, *J. Geodyn*., V. 34, 405-445, 2002.

[4] Sirota, M., et al., The transmitter pointing determination in the Geoscience Laser Altimeter System, *Geophys. Res. Letters*, V. 32, L22S11, doi:10.1029/2005GL024005, 2005.

[5] Luthcke, S., D. Rowlands, T. Williams, and M. Sirota, Reduction of ICESat systematic geolocation errors and the impact on ice sheet elevation change detection, *Geophys. Res. Letters*, V. 32, L21S05,doi:10.1029/2005GL023689, 2005.

[6] Tapley, B., B. Schutz and G. Born, *Statistical Orbit Determination*, Elsevier, 2004.

[7] Schutz, B., J. Zwally, C. Shuman, D. Hancock, J. DiMarzio, Overview of the ICESat Mission, *Geophys. Res. Letters*, V. 32, L21S01, doi: 10.1029/2005GL024009, 2005.

[8] Tapley, B., S. Bettadpur, M. Watkins, C. Reigber, The Gravity Recovery and Climate Experiment: mission overview and early results, *Geophys. Res. Letters*, V. 31, doi:10.1029/2004GL019920, 2004.

[9] Rim, H. TOPEX orbit determination using GPS tracking system, University of Texas at Austin Center for Space Research, Technical Report 92-3, 1992.

[10] Rim, H., S. Yoon, C. Webb, P. Shelus, B. Schutz, ICESat precision orbit determination: solution strategies and accuracy assessment, in review, 2008.

[11] Shuster, M., and S. Oh, Three-axis attitude determination from vector observations, *J. Guidance, Control, and Dynamics*, 4(1), 70-77, 1981.

[12] Lefferts, E. F., F. L. Markley, and M. D. Shuster, Kalman filtering for spacecraft attitude estimation, *J. Guidance, Control, and Dynamics*, 5(5), 417-429, 1982.

[13] Magruder, L., E. Silverberg, C. Webb, and B. Schutz, Pointing and timing validation of the ICESat laser altimeter, *IEEE Trans. in Geoscience and Remote Sensing*, Vol. 45, No. 1, 147-155, Jan. 2007.

[14] Bae, S., C. Webb and B. Schutz, GLAS PAD calibration using Laser Reference Sensor Data, AIAA/AAS Astrodynamics Specialist Conference, Paper AIAA 2004-4857, Aug. 2004.

[15] Bae, S. and B. Schutz, Precision attitude determination using gyro and star tracker data with a batch least-squares estimator, *Advances In the Astronautical Sciences*, Vol. 123, 175-182, Univelt Publishing, 2006.

[16] Abshire, J., et al., Geoscience Laser Altimeter System (GLAS) on the ICESat mission: on-orbit measurement performance, *Geophys. Res. Letters*, Vol. 32, L21S02, doi:10.1029/2005GL024028, 2005.